Mediated resonance effect of the vanadium 3*d* states on phase stability in the Al_8V_5 γ-brass studied by first-principles FLAPW and LMTO-ASA electronic structure calculations

U. Mizutani
Toyota Physical and Chemical Research Institute, Nagakute, Aichi 480-1192, Japan

R. Asahi
Toyota Central R&D Laboratories, Inc., Nagakute, Aichi 480-1192, Japan

H. Sato
Department of Physics, Aichi University of Education, Kariya-shi, Aichi 448-8542, Japan

T. Takeuchi
Ecotopia Science Institute, Nagoya University, Furo-cho, Chikusa-ku, Nagoya 464-8603, Japan
(Received 16 July 2006; revised manuscript received 25 September 2006; published 26 December 2006)

The mechanism for the stability of the Al_8V_5 γ-brass containing 52 atoms in its cubic unit cell has been investigated by means of first-principles full-potential linearized augmented plane wave (FLAPW) and linearized muffin-tin orbital-atomic sphere approximation (LMTO-ASA) electronic structure calculations. The LMTO-ASA identified a deep valley at 0.5 eV above the Fermi level in its density of states (DOS) as arising from orbital hybridizations between V 3*d* and Al 3*p* states. On the other hand, the FLAPW revealed the V 3*d* states mediated resonance of electrons with different sets of lattice planes. The resonance involved is found to be substantial not only at $|\mathbf{G}|^2=18$ or {330} and {411} zones but also at those in the range $14 \leqslant |\mathbf{G}|^2 \leqslant 30$. A comparison with the electronic structure of the CsCl-type AlV compound proved that the V 3*d* states mediated resonance occurs only in Al_8V_5 but not in AlV compound. The V 3*d* states mediated resonance is proved to result in a significant suppression of the *sp*-partial DOS over the energy range from the Fermi level up to +2.2 eV. A gain in the electronic energy has been attributed to the formation of highly condensed bonding states below the Fermi level, again caused by the V 3*d* states mediated resonance. It is also proposed that the Al_8V_5 is stabilized at $e/a=1.94$ rather than 21/13 as is expected from the Hume-Rothery electron concentration rule.

DOI: 10.1103/PhysRevB.74.235119 PACS number(s): 71.20.−b, 81.30.Bx, 71.23.Ft, 71.20.Be

I. INTRODUCTION

There exists a line compound having the composition Al_8V_5 in the Al-V alloy system.[1] As will be described in detail below, its atomic structure is identical to that of the Cu_5Zn_8 γ-brass and is formed by stacking three body-centered cubic (bcc) cells along the *x*, *y*, and *z* directions and subsequently removing the center and corner atoms with slight displacements of remaining atoms, leading to a total of 52 atoms in its cubic unit cell.[2] Indeed, the γ-brass has been recognized for many years as being typical of a structurally complex alloy phase. According to the phase diagram,[1] the V-rich bcc phase exists next to the Al_8V_5 and is extended over the V concentration range from 46 at. % up to pure V. The atomic structures of these two adjacent phases are obviously similar to each other. Hence, we consider a comparison of the electronic structure between these two phases to be important to extract the mechanism of why nature prefers to stabilize a more complicated structure when Al concentration is increased from 54 at. % in the bcc to 61.5 at. % in Al_8V_5.

Brandon *et al.*[3] determined the atomic structure of the Al_8V_5 compound by analyzing the diffraction spectrum measured on a single crystal. They confirmed that it crystallizes into a cubic structure containing 52 atoms in its unit cell with the space group $I\bar{4}3m$, being isostructural to Cu_5Zn_8 known as the prototype "γ-brass."[4,5] It has been established that the γ-brass structure is viewed as being built up by stacking a 26-atom cluster both at the center and the corners of the cubic unit cell with the space group of either $I\bar{4}3m$ or $P\bar{4}3m$.[6] The cluster is known to consist of four, four, six, and 12 atoms at vertices of the inner tetrahedron (IT), outer tetrahedron (OT), octahedron (OH) and cubo-octahedron (CO), respectively. Brandon *et al.*[3] were led to conclude that the IT is occupied by a mixture of two Al and two V atoms, OT only by V atoms, OH by a mixture of two Al and four V atoms, and CO exclusively by 12 Al atoms to conform with the stoichiometric composition Al_8V_5. This is illustrated in Fig. 1(a).

In spite of the possession of different compositions, both Cu_5Zn_8 and Cu_9Al_4 γ-brasses are stabilized at a common electron per atom ratio e/a equal to 21/13 (=1.615) and have been regarded as electron compounds obeying the Hume-Rothery electron concentration rule.[7] Mott and Jones[8] pointed out that the stability of the γ-brass at $e/a=21/13$ can be interpreted within the free electron model by assuming that a spherical Fermi surface totally touches 36 zone planes originating from sets of 24-fold {411} and 12-fold {330} lattice planes unique to the γ-brass structure. They also noted that an increase in electron concentration from $e/a=3/2$, at which the bcc phase is stabilized, to 21/13 acts in favor of the γ-brass structure. Obviously, the resonance of electrons at the Fermi level with sets of lattice planes is enhanced from

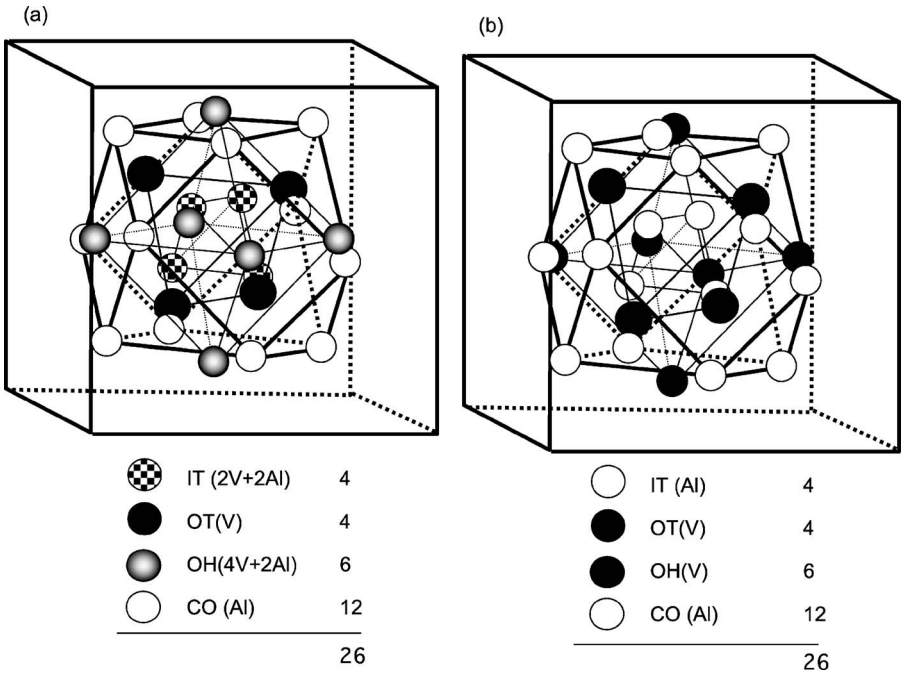

FIG. 1. (a) Experimentally determined atomic structure of Al_8V_5 γ-brass (Ref. 3) and (b) chemical disorder-free model employed in the present electronic structure calculations.

12 in bcc to 36 directions in the γ-brass as a result of an increase in the number of the relevant Brillouin zone planes.

The electronic specific heat coefficient in the γ-brass has been reported to decrease very sharply with increasing the electron concentration e/a.[9] This unique behavior was interpreted by assuming that the Fermi surface has touched the {330} and {411} zone planes and that the Fermi level in the γ-brass falls on a declining slope of the density of states (hereafter abbreviated as DOS) curve. The location of the Fermi level on the sharply declining slope of the DOS, which is now called the pseudogap, has been universally observed in quasicrystals and their approximants and is believed to play a crucial role in stabilizing such a structurally complex structure.[10] However, earlier interpretations based on the free electron model are obviously too oversimplified to draw a decisive conclusion about the stability mechanism, since it is unable to reproduce the pseudogap structure in the DOS.

Attempts beyond such qualitative discussions for the γ-brass were first made by Paxton *et al.*,[11] who performed first-principles LMTO-ASA (linearized muffin-tin orbital-atomic sphere approximation) electronic structure calculations for the Cu_5Zn_8 γ-brass. Mizutani *et al.*[12] discussed the formation of the pseudogap across the Fermi level in terms of both *sp-d* hybridization and the Fermi surface–Brillouin zone (hereafter abbreviated as FsBz) interaction by analyzing the electronic structure calculated from the LMTO-ASA method for the Cu_5Zn_8. Soon after that, we realized that, rather than the LMTO-ASA, FLAPW (full-potential linearized augmented plane wave) electronic structure calculations should be more straightforward to extract the FsBz interaction, since the self-consistent eigenfunction is cast into plane waves summed over reciprocal lattice vectors in the interstitial region outside the muffin-tin (hereafter abbreviated as MT) potential.[10,13–15]

Asahi *et al.*[13] performed the FLAPW electronic structure calculations for both Cu_5Zn_8 and Cu_9Al_4 γ-brasses to clarify the origin of the existing pseudogap across the Fermi level. They calculated the sum of squared coefficients, $\Sigma_{\{hkl\}}|C_{hkl}|^2$, over equivalent zones $\{hkl\}$ of the wave function outside the MT potential at the symmetry point N at energies sustaining the pseudogap near the Fermi level and plotted it against the sum of squared Miller indices $h^2+k^2+l^2$ or square of reciprocal lattice vector $|\mathbf{G}|^2$ in units of $(2\pi/a)^2$, where a is the lattice constant. It turned out that, only when $|\mathbf{G}|^2=18$ corresponding to the {330} and {411} zone planes, the value of $\Sigma_{\{hkl\}}|C_{hkl}|^2$ for both Cu_5Zn_8 and Cu_9Al_4 becomes extremely large for both the highest occupied and lowest unoccupied states responsible for the formation of the pseudogap. It was further shown that electrons near the Fermi level exclusively resonate with the set of lattice planes {330} and {411}, resulting in cos- and sin-type stationary waves and, in turn, the pseudogap. This was indeed the attempt beyond the nearly free-electron (NFE) model and was successfully applied for realistic systems, where the Cu 3*d* states form a more localized band immediately below the Fermi level.[10,13–15]

Asahi *et al.*[14] further extended their approach to the TM_2Zn_{11} (TM=Pd, Ni, Co, and Fe) γ-brasses containing the transition metal element TM with the intent to test if the pseudogap is formed, regardless of the atomic species TM, and if the $|\mathbf{G}|^2=18$ resonance is again responsible for its formation. They found it to be true for both Ni_2Zn_{11} and Pd_2Zn_{11} but to collapse in Co_2Zn_{11} and Fe_2Zn_{11}, where the pseudogap is shifted above the Fermi level. This suggested the presence of a different stabilization mechanism in the latter two, even though they equally crystallize into the same complex structure as the prototype Cu_5Zn_8.

The present work is carried out to gain deeper insight into why the Al_8V_5 γ-brass, which involves the early transition metal element V as a partner to Al, is stabilized by crystallizing into the same complex structure as Cu_5Zn_8. Remember that the smaller its atomic number in the 3*d* element of the periodic table is, the more the center of gravity of the *d* band

towards the Fermi level is shifted and, hence, the more complex the evaluation of the Hume-Rothery electron concentration rule would be. We attempted to explain why an increase in the number of atoms in a unit cell is needed to stabilize the Al_8V_5 compound relative to the bcc phase by comparing its electronic structure with that of the hypothetical CsCl-type AlV compound, which contains only two atoms in its cubic cell. We also focus on whether the Hume-Rothery electron concentration rule, according to which the γ-brass structure would be stabilized, still plays a key role for the system, where the V 3*d* band dominates the DOS near the Fermi level. As a second objective, we have evaluated the effective e/a value for the Al_8V_5 γ-brass to examine if the Hume-Rothery electron concentration rule claiming the γ-brass structure to be stabilized at $e/a=21/13$, is universal or not.

II. ATOMIC STRUCTURE

A. Al_8V_5 γ-brass

As mentioned in the Introduction, chemical disorder exists in the experimentally determined atomic structure of the Al_8V_5 γ-brass.[3] We consider this disorder in Al_8V_5 to be unavoidable, since the γ-brass is formed through a peritectic reaction at temperatures higher than 1670 °C.[1] Nevertheless, the ground state at absolute zero would be free from such chemical disorder to fulfill with the third law of thermodynamics.

Chemical disorder must also be avoided in first-principles electronic structure calculations. A chemical disorder-free structure is constructed for the electronic structure calculations by minimizing departure from the experimentally derived structure. The structure is simplified in such a way that IT, OT, OH, and CO are exclusively occupied by four Al, four V, six V, and 12 Al atoms in the 26-atom cluster, respectively, without altering the composition Al_8V_5. The chemical disorder-free model thus constructed is shown in Fig. 1(b) in comparison with the experimentally determined one in Fig. 1(a). The lattice constant of 9.223 A is employed.[3]

B. CsCl-type AlV compound

The FLAPW electronic structure calculations were also performed for a hypothetical equiatomic compound AlV with the CsCl-type ordered structure. The lattice constant $a=3.078$ A was chosen by extrapolating the V concentration dependence of the lattice constant available in literature for the bcc phase.[16]

III. FIRST-PRINCIPLES ELECTRONIC STRUCTURE CALCULATIONS

A. LMTO-ASA method

The LMTO-ASA electronic structure calculations provide decisive information about the role of orbital hybridizations with computational efficiency and are performed in the periodic zone scheme in combination with the local density functional theory. The potential parameters are self-consistently determined at 285 independent **k** points in the irreducible wedge of the Brillouin zone for the Al_8V_5 γ-brass.[17,18] The hybridization terms between the V 3*d* and Al 3*p* states are intentionally deleted to examine how orbital hybridizations between the neighboring constituent elements affect the band structure. The effect of orbital hybridizations between the V 3*d* and Al 3*p* states on the electronic structure was also studied for the CsCl-type AlV compound.

B. FLAPW method

The details of the present FLAPW electronic structure calculations have been described elsewhere.[13] Briefly, the wave function is expressed as

$$\psi_i(\mathbf{r},\mathbf{k}) = \sum_{\mathbf{G}} C^i_{\mathbf{k}+\mathbf{G}} \phi(\mathbf{r},\mathbf{k}+\mathbf{G}), \tag{1}$$

where **k** is an arbitrary wave vector in the irreducible Brillouin zone, **G** is a reciprocal lattice vector, and i is the band index. Here the basis functions are given as[19,20]

$$\phi(\mathbf{r},\mathbf{k}+\mathbf{G}) = \begin{cases} \Omega^{-1/2} e^{i(\mathbf{k}+\mathbf{G})\cdot\mathbf{r}}, & r \in \text{interstitial}, \\ \sum_{lm} [A^\alpha_{lm}(\mathbf{k}+\mathbf{G}) u_l(E^\alpha_l, r_\alpha) + B^\alpha_{lm}(\mathbf{k}+\mathbf{G}) \dot{u}_l(E^\alpha_l, r_\alpha)] Y_{lm}(\hat{r}_\alpha), & r \in \text{sphere}, \end{cases} \tag{2}$$

where $u(E^\alpha_l, r_\alpha)$ and $\dot{u}_l(E^\alpha_l, r_\alpha)$ are solutions of the radial Schrödinger equation solved at a fixed energy E^α_l and their derivatives, respectively, $Y_{lm}(\hat{r}_\alpha)$ is a spherical harmonics, and the coefficients $A^\alpha_{lm}(\mathbf{k}+\mathbf{G})$ and $B^\alpha_{lm}(\mathbf{k}+\mathbf{G})$ are determined by the requirement that the plane waves and their radial derivatives are continuous at the surface of the atomic spheres. The number of plane waves was about 2900 in the present Al_8V_5 γ-brass. The electronic structure was also calculated for the CsCl-type AlV compound.

IV. DISCUSSION

A. Extraction of orbital hybridization effect

Figure 2(a) shows the LMTO-ASA-derived DOS for the Al_8V_5 γ-brass. It has a deep pseudogap at about 0.5 eV above the Fermi level. To study its origin, we calculated the DOS without the contribution from orbital hybridizations between the V 3*d* and Al 3*p* states. As shown in Fig. 2(b), the pseudogap has essentially disappeared. This means that the V 3*d* states are split into bonding and antibonding states caused

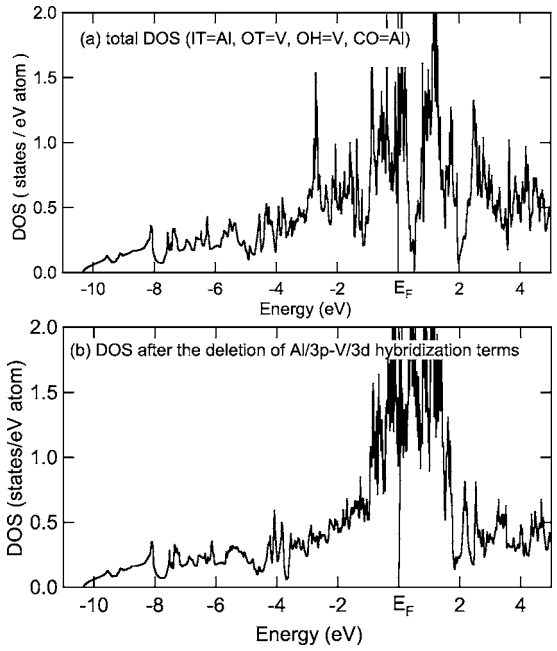

FIG. 2. (a) LMTO-ASA-derived total DOS and (b) the DOS associated with no hybridization terms between V 3*d* and Al 3*p* in the LMTO-ASA basis functions for the Al_8V_5 γ-brass. The deep pseudogap at 0.5 eV above the Fermi level has disappeared after zeroing orbital hybridizations.

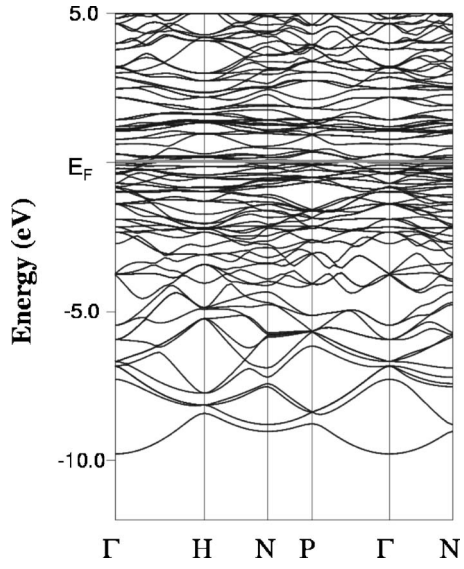

FIG. 3. Dispersion relations derived from FLAPW electronic structure calculations for the Al_8V_5 γ-brass.

by orbital hybridizations with the Al 3*p* states. Hence, this is equally expected to occur in the CsCl-type AlV compound. Indeed, a deep pseudogap is found at about 2 eV above the Fermi level in AlV, as will be shown in Fig. 10(a). However, it must be noted that the pseudogap above the Fermi level cannot contribute to the stabilization of this complex structure. Hence, we need to explore other origins for the stabilization mechanism.

B. Extraction of resonance effect with sets of lattice planes

The energy dispersion relations calculated from the FLAPW method for the Al_8V_5 γ-brass are shown in Fig. 3. As mentioned above, the corresponding DOS is included in Fig. 10(a). The densely populated states over the range −3 to +3 eV in the dispersion relations can be well ascribed to the V 3*d* states. It is apparently separated into the bonding and antibonding states by a sparse region, i.e., the pseudogap discussed above at about 0.5 eV above the Fermi level. Indeed, the FLAPW-derived DOS in Fig. 10(a) is well consistent with the LMTO-derived one in Fig. 2(a).

To begin with, the $|\mathbf{G}|^2$ dependence of a squared coefficient $\Sigma_{\{hkl\}}|C_{hkl}|^2$ summed over equivalent zones $\{hkl\}$ of the wave function outside the MT potential, i.e., the Fourier spectrum of plane wave components is calculated at six different energy eigenstates at the symmetry point *N*. The results are shown in Fig. 4. At the energy of −7.41 eV, the Fourier component is extremely strong only at $|\mathbf{G}|^2=6$ corresponding to {211} zone planes. The intensity ratio of the strongest peak over the next strongest one, $I_{G^2=6}/I_{\text{next}}$, turns out to be 59. The exclusive contribution due to $|\mathbf{G}|^2=6$ at this energy can be easily understood from Fig. 3, where free electron-like states are split into bonding and antibonding states and open a small energy gap across the {211} zone planes.

The Fourier spectrum, when the energy is increased, is spread more widely over a wide range of $|\mathbf{G}|^2$. This is due certainly to mixing with wave functions originating from more localized V 3*d* states. But it is interesting to note that the component at $|\mathbf{G}|^2=18$ is always significant for all energies studied, though the intensity ratio $I_{G^2=18}/I_{\text{next}}$ is suppressed below 15. This means that the resonance of electrons extending outside the MT potential with sets of lattice planes {411} and {330} is occurring in all energies, over which the V 3*d* states are spread. This is in sharp contrast to the previous findings that the $|\mathbf{G}|^2=18$ resonance occurs only at energies sustaining the pseudogap in γ-brasses like Cu_5Zn_8 and Cu_9Al_4, where Cu 3*d* states have little to do with the formation of the pseudogap.[13] Thus, we note that the $|\mathbf{G}|^2=18$ resonance is important but those in the range $|\mathbf{G}|^2 \geqslant 14$ are also equally important in the Al_8V_5.

The energy dependence of the coefficient $\Sigma_{\{hkl\}}|C_{hkl}|^2$ at selected values of $|\mathbf{G}|^2$ at the point *N* is plotted in Fig. 5. As is expected, peaks are well centered in a narrow energy range, when $|\mathbf{G}|^2$ is lower than 10, since electronic states are hardly perturbed by the V 3*d* states. However, the spectrum begins to widen and be split into two peaks, i.e., one below and the other above the Fermi level, as $|\mathbf{G}|^2$ increases beyond 14. This is interpreted as the formation of bonding and antibonding states caused by the resonance of more itinerant electrons with a set of lattice planes specified by the reciprocal lattice vector **G** in the energy range, where the V 3*d* states coexist. Indeed, the bonding and antibonding states are widely separated as if they were repelled by the V 3*d* states. As a result, the Fermi level is located at the position where only the bonding states are filled. This implies that V 3*d* states would serve to mediate the resonance of more mobile electrons with sets of lattice planes and play a key role in

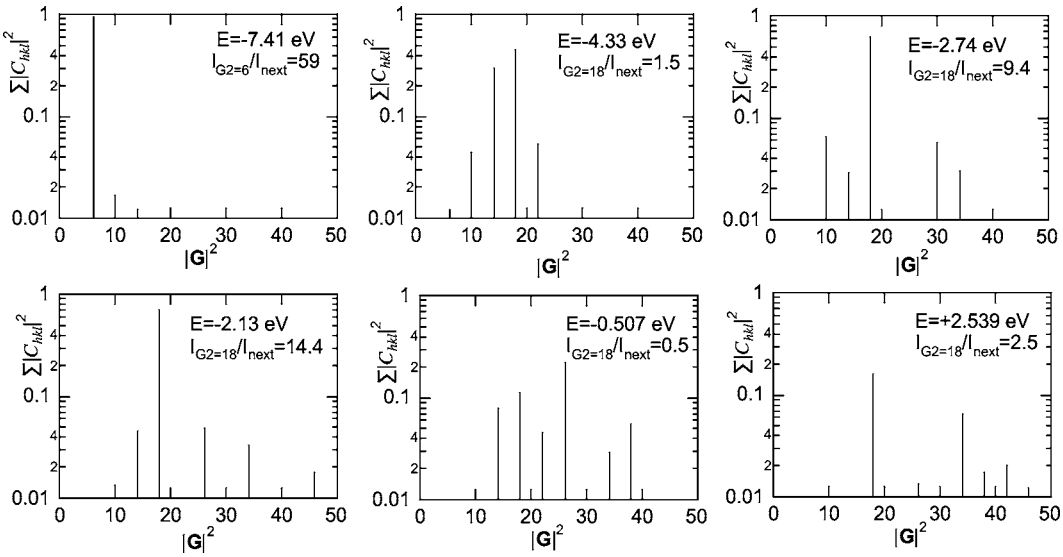

FIG. 4. $|\mathbf{G}|^2$ dependence of $\Sigma_{\{hkl\}}|C_{hkl}|^2$ of the FLAPW wave function outside the MT potential at energy eigenvalues of −7.41, −4.33, −2.74, −2.13, −0.507, and +2.539 eV at the symmetry point N in Fig. 3. The ordinate is on a logarithmic scale. At energy of −7.41 eV, the ratio $I_{\mathbf{G}2=6}/I_{\text{next}}$ refers to the intensity at $|\mathbf{G}|^2=6$ over the next strongest one, i.e., $|\mathbf{G}|^2=10$ in this case. Otherwise, the ratio $I_{\mathbf{G}2=18}/I_{\text{next}}$ refers to the intensity at $|\mathbf{G}|^2=18$ over the next strongest one.

gaining the electronic energy to stabilize the Al_8V_5 γ-brass structure.

To elucidate more the origin of the V 3*d* states mediated resonance, we calculated two different population-weighted electronic energies U_{av} and U_{oc} defined below at different values of $\mathbf{G}$ at the three symmetry points N, H, and Γ in the reduced Brillouin zone:

$$U_{av}(\mathbf{G}) = \frac{\sum_{E=E_0}^{\infty} |C_{\mathbf{G}}(E)|^2 E}{\sum_{E=E_0}^{\infty} |C_{\mathbf{G}}(E)|^2} \tag{3}$$

and

$$U_{oc}(\mathbf{G}) = \frac{\sum_{E=E_0}^{E_F} |C_{\mathbf{G}}(E)|^2 E}{\sum_{E=E_0}^{E_F} |C_{\mathbf{G}}(E)|^2}, \tag{4}$$

where E_0 refers to the bottom of the valence band. Equation (3) represents the electronic energy averaged over both bonding and antibonding states extended from E_0 to infinity, whereas Eq. (4) defines the electronic energy averaged only over occupied states. Both U_{av} and U_{oc} thus calculated are plotted in Fig. 6 as functions of the square of the reciprocal lattice vector $|\mathbf{G}|^2$ along with the free electron line drawn so as to meet the value of E_{av} at $|\mathbf{G}|^2=0$.

The value of U_{av} is found to agree well with the free electron line up to about $|\mathbf{G}|^2=10$ but begins to gradually deviate downwards with further increase in $|\mathbf{G}|^2$. Both the free electron line and U_{av} cross the Fermi level at $|\mathbf{G}|^2=21$ and 22.5, respectively. On the other hand, U_{oc} remains low relative to U_{av} up to the Fermi level. This is certainly caused by the fact that antibonding states appearing above the Fermi level are not counted in the calculation of U_{oc}. In other words, we consider the difference $U_{av}-U_{oc}$ to reflect the gain in the electronic energy due to the splitting into bonding and antibonding states, though the energy is evaluated only at specific symmetry points in the Brillouin zone. It is, therefore, worthwhile noting that both U_{av} and U_{oc} in Fig. 6 fall

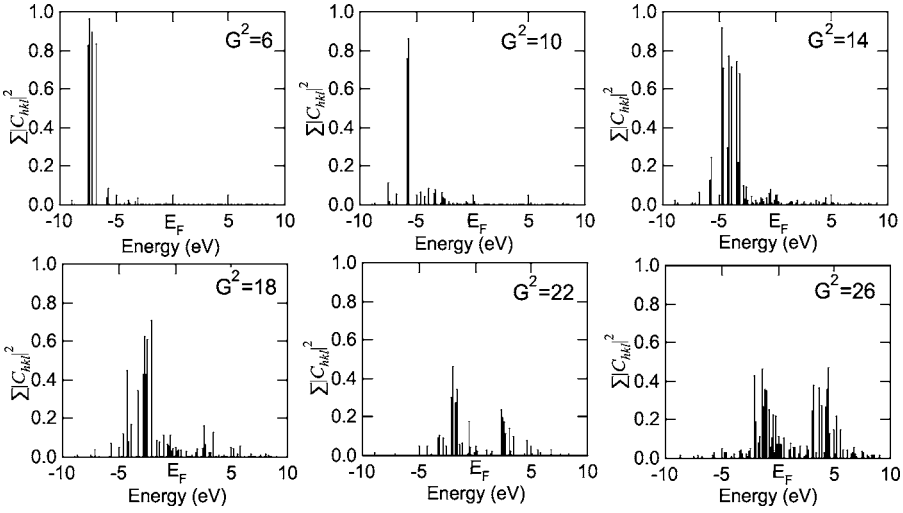

FIG. 5. Energy dependence of $\Sigma_{\{hkl\}}|C_{hkl}|^2$ at selected values of $|\mathbf{G}|^2$ at the point N for the Al_8V_5 γ-brass. Note that the splitting into bonding and antibonding states is observed for all values of $|\mathbf{G}|^2$ over the range 14–30.

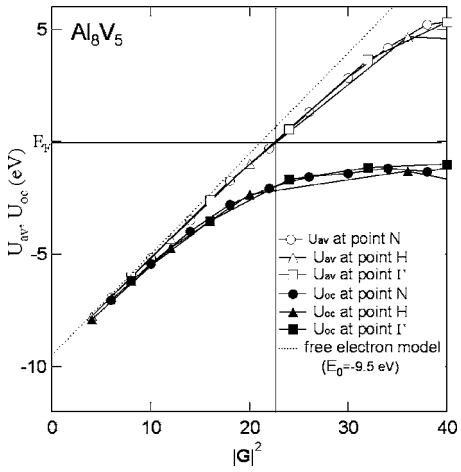

FIG. 6. $|\mathbf{G}|^2$ dependence of the electronic energies U_{av} and U_{oc} calculated from Eqs. (3) and (4) at the points N, H, and Γ for the Al_8V_5 γ-brass, respectively.

on the universal curve within resolution, regardless of the choice of the three symmetry points N, H, and Γ.

The squared Fourier coefficient is summed over all occupied states below the Fermi level, $\Sigma_{E_0}^{E_F}\Sigma_{\{hkl\}}|C_{hkl}(\mathbf{G},E)|^2$, at a fixed value of $|\mathbf{G}|^2$ at the point N for the Al_8V_5. Its $|\mathbf{G}|^2$ dependence is shown in Fig. 7. One can clearly see a large enhancement in the plane-wave components over the range $14 \leqslant |\mathbf{G}|^2 \leqslant 30$. This indicates that momentum transfer mediated by more localized V $3d$ states is substantial in this $|\mathbf{G}|^2$ range. Its unique $|\mathbf{G}|^2$ dependence is apparently reflecting the multiplicity of equivalent lattice planes: $|\mathbf{G}|^2=14$, 18, 22, and 26 correspond to 48-fold {321}, 36-fold {411} plus {330}, 24-fold {332}, and 72-fold {431} plus {510} zones, respectively.

C. Electronic structure calculations for the hypothetical CsCl-type AlV compound

As mentioned in the Introduction, the bcc phase is stable down to 46 at. % V at high temperatures around 1670 °C in the Al-V phase diagram.[1] An AlV alloy with equiatomic

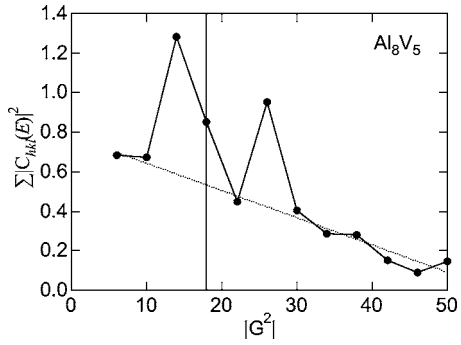

FIG. 7. $|\mathbf{G}|^2$ dependence of the squared coefficient summed over both equivalent $\{hkl\}$ planes and all occupied states below the Fermi level, $\Sigma_{E_0}^{E_F}\Sigma_{\{hkl\}}|C_{hkl}(\mathbf{G},E)|^2$, for the Al_8V_5 γ-brass. An enhancement in the plane-wave components is found over the range $14 \leqslant |\mathbf{G}|^2 \leqslant 30$.

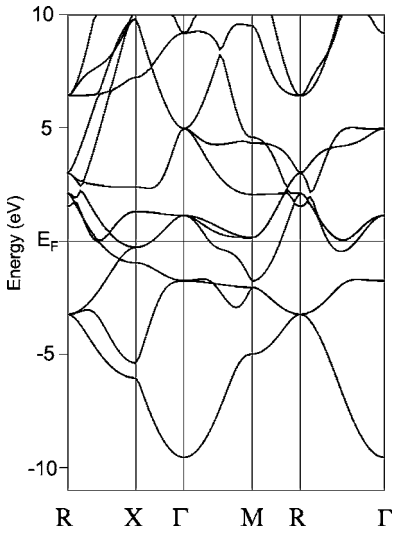

FIG. 8. Dispersion relations derived from FLAPW electronic structure calculations for the CsCl-type AlV compound.

composition may be stable at high temperatures in the range 1440–1740 °C. Upon lowering temperature, it will decompose into the bcc phase with less V concentration and Al_8V_5. Hence, the AlV bcc phase will no longer be stable at absolute zero. We nevertheless performed the FLAPW electronic structure calculations for a hypothetical equiatomic compound AlV with the CsCl-type ordered structure to examine how the resonance effect discussed in Sec. IV B for the Al_8V_5 changes when the number of atoms in a unit cell is reduced from 52 to two.

Figure 8 shows the FLAPW-derived energy dispersion relations for the AlV compound. The corresponding DOS is also included in Fig. 10(a). We have also performed the LMTO-ASA electronic structure calculations for the AlV compound and obtained results consistent with those derived from the FLAPW method. Briefly, the deletion of V-$3d$–Al-$3p$ hybridization terms substantially narrowed the V $3d$ band in the energy range from −1.6 to +1.9 eV and disintegrated hump structures in the sp-partial DOS, which will be further discussed in Sec. IV D.

The squared coefficient $\Sigma_{\{hkl\}}|C_{hkl}|^2$ summed over equivalent zones $\{hkl\}$ of the wave function outside the MT potential is plotted in Fig. 9(a) on a logarithmic scale as a function of $|\mathbf{G}|^2$ at three different energy eigenvalues at the symmetry point M. As far as energies below the Fermi level are concerned, values of $\Sigma_{\{hkl\}}|C_{hkl}|^2$ higher than 0.01 are distributed only in $|\mathbf{G}|^2$ lower than 10. This is in sharp contrast to the data in Fig. 4 for Al_8V_5, where those in the range $|\mathbf{G}|^2 \geqslant 14$ are substantial. This obviously reflects the difference in the size of the unit cell between the two phases.

In a way similar to Fig. 5, the energy spectrum of $\Sigma_{\{hkl\}}|C_{hkl}|^2$ is plotted in Fig. 9(b) at different $|\mathbf{G}|^2$ values for the AlV compound. Note that each spectrum represents the energy distribution of the electron wave at a fixed $|\mathbf{G}|^2$. For example, the energy spectrum at $|\mathbf{G}|^2=2$ at point M is viewed as splitting into bonding and antibonding states across 12-fold {110} zone planes. Such splitting is found to hold for $|\mathbf{G}|^2=4$ or {200} zone planes at point Γ, $|\mathbf{G}|^2=1$ and

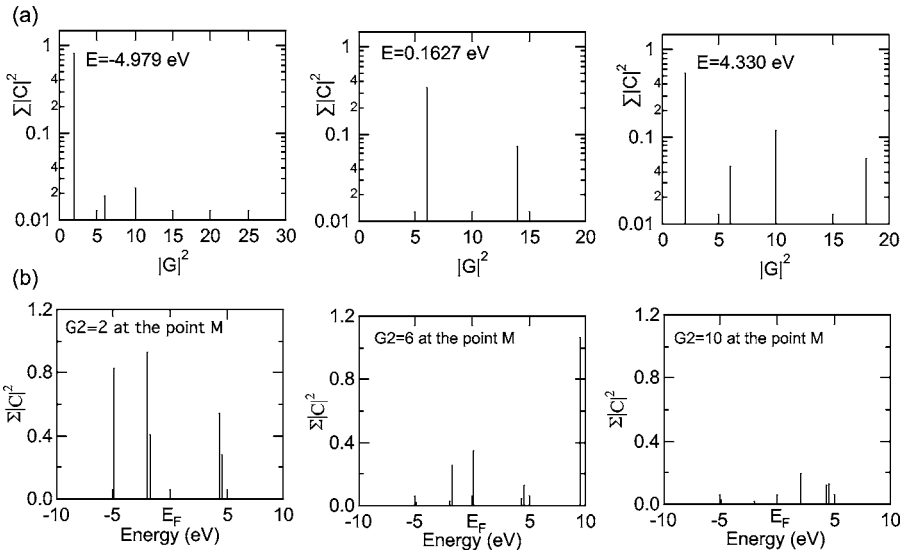

FIG. 9. (a) $|\mathbf{G}|^2$ dependence of $\Sigma_{\{hkl\}}|C_{hkl}|^2$ of the FLAPW wave function outside the MT potential at energy eigenvalues of −4.979, 0.1627, and 4.330 eV at point *M* in Fig. 8 for the AlV compound. (b) Energy dependence of $\Sigma_{\{hkl\}}|C_{hkl}|^2$ at $|\mathbf{G}|^2=2$, 6, and 10 at point *M* for the AlV compound.

5 at point *X*, and $|\mathbf{G}|^2=3$ at point *R*. However, the "bonding states" thus formed are certainly far less populated than those at point *N* for Al_8V_5 shown in Fig. 5. Hence, the energy spectrum for AlV in Fig. 9(b) differs qualitatively from that for Al_8V_5 in Fig. 5.

D. Comparison of total and partial DOS between Al_8V_5 and AlV

Figures 10(a)–10(c) represent the total, *d*-partial, and *sp*-partial DOS calculated from the FLAPW method for both the Al_8V_5 and AlV compounds. First, we direct our attention to the total DOS. The overall features in the total DOS are similar to each other in the sense that the V 3*d* band spreads from −3 to +3 eV and is split into bonding and antibonding states with the deep valley +2 eV above the Fermi level. However, the DOS in AlV is no longer spiky because of great reduction in foldings in energy dispersions as a result of the existence of only two atoms in the unit cell.

Some caution is needed when the FLAPW-derived partial DOS is discussed. As is clear from Eq. (2), the wave function is expanded into partial waves inside the MT potential but into plane waves outside it. The partial DOS is calculated from the wave functions inside the MT potential. Hence, the *sp*-partial DOS thus obtained would not quantitatively reproduce that of *sp*-electrons extending widely in the interstitial region. The situation in the *d*-partial DOS is better, since it largely represents the V 3*d* states mostly residing inside the MT potential. As a matter of fact, the sum of *sp*- and *d*-partial DOS does not reproduce the most accurate total DOS.

The total electron concentration including both *sp*- and *d*-electrons per atom, N_{total}, and the electronic energy per atom, U_{total}, may be calculated by integrating the total DOS,

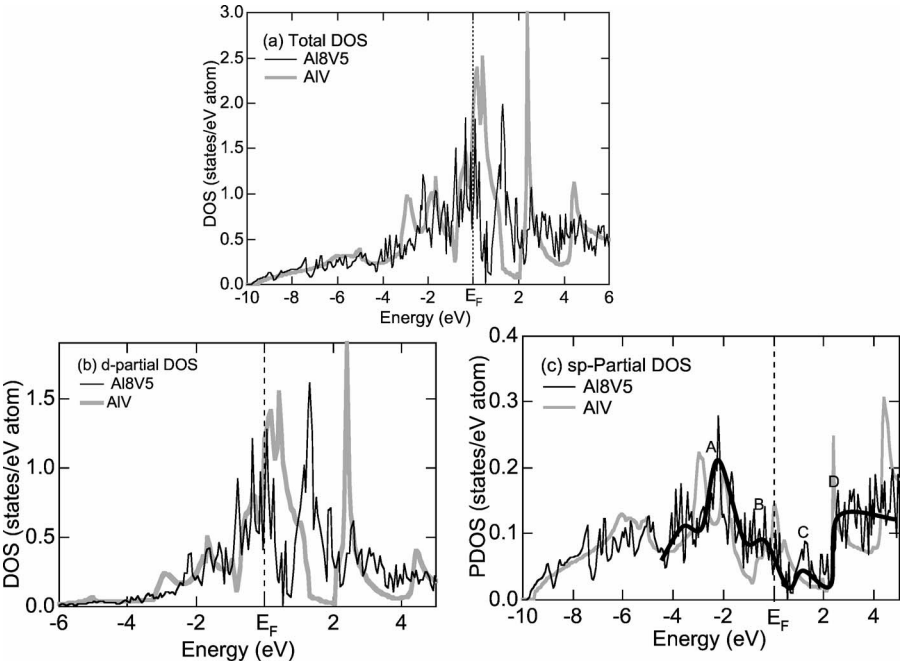

FIG. 10. (a) Total DOS, (b) *d*-partial DOS, and (c) *sp*-partial DOS calculated from FLAPW for Al_8V_5 (thin black) and AlV (thick gray) compounds. The *d*-partial DOS for AlV shown in (b) is multiplied by the factor 10/13 to allow a direct comparison with the *d*-partial DOS for Al_8V_5. The thick black line in (c) approximates the *sp*-partial DOS of Al_8V_5 after smoothing. "A" and "D" refer to the edges of the pseudogap, "B" and "C" the plateau and hump inside the pseudogap, respectively.

$D_{\text{total}}(E)$, from the bottom of the valence band E_0 up to the Fermi level:

$$N_{\text{total}} = \int_{E_0}^{E_F} D_{\text{total}}(E)dE \tag{5}$$

and

$$U_{\text{total}} = \int_{E_0}^{E_F} D_{\text{total}}(E)EdE. \tag{6}$$

The value of N_{total} turned out to be 3.77 and 4.04 electrons per atom for Al_8V_5 and AlV, respectively, being consistent with the fact that V and Al donate five and three electrons per atom to form the valence band. The respective electronic energies U_{total} thus deduced are 26.6 and 29.0 eV/atom, indicating that the Al_8V_5 γ-brass apparently possesses a lower electronic energy. But a straightforward conclusion about stability cannot be drawn from this, since we are comparing two phases at different alloy compositions.

As noted above, the *d*-partial DOS mainly reflects the V 3*d* states inside the MT potential. Since the V concentration for AlV is 10/13 times as large as that in the Al_8V_5, the *d*-partial DOS for AlV shown in Fig. 10(b) is shown after multiplying the DOS by this factor. As far as the DOS below the Fermi level is concerned, they are quite similar, though the spiky structure is lost in AlV. Instead, the *d*-partial DOS above the Fermi level is sharply different between them: the DOS for the Al_8V_5 is much smaller than that for the AlV in the energy range up to about +1 eV because of the presence of the deep pseudogap centered at +0.5 eV in the former. Hence, even a small change in the position of the Fermi level relative to peaks in the *d*-partial DOS for both phases might delicately affect phase stability, though unoccupied states above the Fermi level do not contribute to the electronic energy.

We consider the effect of the *sp*-partial DOS on stability to be more important and focus on V 3*d* mediated resonance effects. Since the *sp*-partial DOS in Al_8V_5 is spiky, it may be smoothed as shown in Fig. 10(c) with a thick curve. The smoothed *sp*-partial DOS is characterized by a deep pseudogap sandwiched by its boundaries at −2.2 [marked as "A" in Fig. 10(c)] and +2.2 eV ("D") with a plateau marked as "B" and a small hump "C." Note that a slope from "A" through "B" to "C" is steep but finite whereas that at "D" is almost infinite. On the other hand, the *sp*-partial DOS in the AlV compound exhibits a rather large hump across the Fermi level.

Though energy spectra of $\Sigma_{\{hkl\}}|C_{hkl}|^2$ were already shown in Fig. 5, we show in Fig. 11 all the spectra over the range $6 \leqslant |\mathbf{G}|^2 \leqslant 50$ at the point *N* for the Al_8V_5 γ-brass without differentiating its $|\mathbf{G}|^2$ dependence. The *d*-partial DOS shown in Fig. 10(b) is superimposed. The separation into bonding and antibonding states due to the V 3*d* states mediated resonance is now much clearer with an apparent band gap of 2 eV located immediately above the Fermi level. The number of states there should be heavily suppressed in spite of the existence of a high *d*-partial DOS. This means that mobile *sp*-electrons must be very limited in this energy range, at least, at the symmetry point *N* we studied. The *sp*-partial

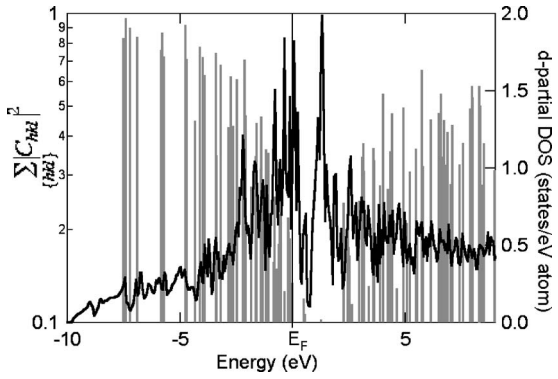

FIG. 11. All energy spectra of $\Sigma_{\{hkl\}}|C_{hkl}|^2$ are plotted without differentiating the $|\mathbf{G}|^2$ dependence over the range $6 \leqslant |\mathbf{G}|^2 \leqslant 50$ for the Al_8V_5 γ-brass. The *d*-partial DOS shown in Fig. 10(b) is superimposed. A scarcely populated window opens in the energy region from the Fermi level up to 2.2 eV in spite of the presence of a large *d*-partial DOS.

DOS, however, is not strictly zero but even a small hump "C" remains in Fig. 10(c). This may represent the contribution from regions other than around point *N* in the Brillouin zone. Another point to be emphasized in Fig. 11 is that the bonding state is densely populated immediately below the Fermi level and gives rise to a steep negative slope from "A" up to the Fermi level in the *sp*-partial DOS in Fig. 10(c). The hump across the Fermi level in the AlV compound is essentially wiped out and replaced by a less structured declining slope with a plateau "B" in Al_8V_5 as a result of the V 3*d* mediated resonance coupled with an increased zone folding.

A phase competition between the γ-brass and AlV may still be delicate, based on a quick inspection of the two *sp*-partial DOSs shown in Fig. 10(c). But, a gain in the electronic energy has been evidenced not only from Fig. 6 but also from Fig. 11, where bonding states caused by the V 3*d* states mediated resonance are highly condensed below the Fermi level. We believe this to play a critical role for explaining the stability of the complex γ-brass structure.

E. Determination of the effective *e*/*a* for the V atom in Al_8V_5

First of all, the Fermi level in the Al_8V_5 and AlV compounds is determined by filling $(4s)^2(3d)^2$ electrons from the V atom and $(3s)^2(3p)$ electrons from Al atoms into the valence band. Thus, an increase in the V concentration increases the total number of electrons per atom, N_{total}, as defined by Eq. (5). On the other hand, the Hume-Rothery electron concentration rule counts only *sp*-electrons per atom in the valence band, which is often denoted as *e*/*a*. For example, the *e*/*a* value of pure Cu is unity, though N_{total} is 11.

Figures 12(a) and 12(b) show the dispersion relations along the $\Gamma N \Gamma$ direction for the Al_8V_5 γ-brass in the free electron model and the one derived after ignoring the hybridization terms between V 3*d* and all other states including Al 3*s*, Al 3*p*, V 4*s*, V 4*p*, and V 3*d* in the LMTO-ASA electronic structure calculations, respectively. In the latter, the V 3*d* states are isolated as a level at 0.73 eV above the Fermi level and, hence, may be regarded as a "nearly free electron"

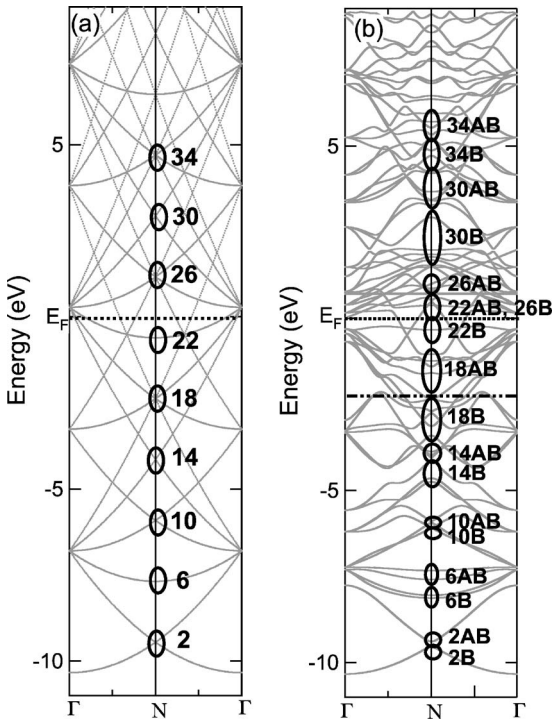

FIG. 12. Energy dispersion relations along ΓNΓ directions in (a) the free-electron model and (b) the nearly free-electron model, where hybridization terms of V 3*d* with all other states are neglected in the LMTO-ASA method for the Al_8V_5 γ-brass. The degenerate states at point *N* are easily identified in terms of $|\mathbf{G}|^2$ in (a). Zones splitting giving rise to bonding (B) and antibonding (AB) states in (b) are assigned by using (a) as a guide.

model. Its comparison with the free electron model allows us to index bonding (marked as B) and antibonding (marked as AB) states caused by the zone splitting in terms of $|\mathbf{G}|^2$ at point *N*, as shown in Fig. 12(b). The electronic states near the Fermi level are found to be most heavily perturbed by the resonance with $|\mathbf{G}|^2=22$ and 26. Instead, the $|\mathbf{G}|^2=18$ resonance occurs in the energy range −1.6 to −2.6 eV below the Fermi level, as can be seen from the dotted-dashed line drawn in Fig. 12(b).

The total DOS is calculated from the dispersion relations in Fig. 12(b) and is shown in Fig. 13. The pseudogap is located in the energy range −2.4 to −1.6 eV. This is safely attributed to the resonance of *sp* electrons with a set of lattice planes with $|\mathbf{G}|^2=18$. Indeed, the electron concentration close to 21/13 is obtained at the center of the pseudogap, as indicated by the arrow in Fig. 13. Thus, this reproduces well the electronic structure obtained for the prototype γ-brass like Cu_5Zn_8.[13] It is to be emphasized that the electron concentration in Al_8V_5 must be higher than 21/13, since the Fermi level is located about 2 eV higher than the energy at which the $|\mathbf{G}|^2=18$ resonance occurs. Indeed, the electron concentration of 2.19 is obtained at the Fermi level. However, we are well aware that the derivation given above is oversimplified, since the V 3*d* state and its interaction with all other states are fully ignored. More elaborate arguments are required to assess more reliably the *e*/*a* value for the Al_8V_5 γ-brass.

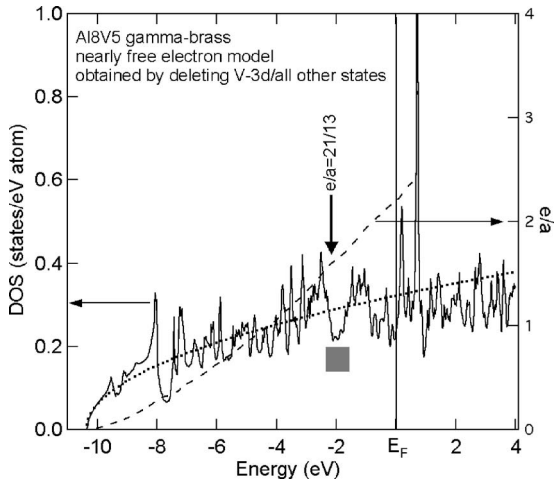

FIG. 13. The total DOS calculated from the dispersion relations shown in Fig. 12(b) for the Al_8V_5 γ-brass. The pseudogap centered at −2 eV is easily identified as originating from the resonance with set of lattice planes specified by $|\mathbf{G}|^2=18$ and the *e*/*a* value of 21/13 is obtained by integrating the DOS up to the middle of this pseudogap.

Asahi *et al.*[14] proposed a new method to evaluate the *e*/*a* value for the γ-brass involving a transition metal element as a partner element by constructing a single-branch energy dispersion relation in the extended zone scheme. The value of $2(\mathbf{k}_i+\mathbf{G})$ giving the largest Fourier component was first deduced from the Fourier spectrum of the FLAPW wave function at a given energy eigenvalue, where $\mathbf{k}_i$ is selected at 200 points in the irreducible wedge corresponding to 1/48 of the reduced Brillouin zone. The quantity $k_G(E)$ is defined as

$$2k_G(E) \equiv 2\sum_{i=1}^{N} \omega_i |\mathbf{k}_i + \mathbf{G}|_E, \tag{7}$$

where *i* runs over the $\mathbf{k}_i$ points mentioned above, ω_ι is the weight associated with each $\mathbf{k}_i$ point, and $|\mathbf{k}_i+\mathbf{G}|_E$ is evaluated at the energy *E* by linearly interpolating between energy eigenvalues. The energy dependence of $\{2k_G(E)\}^2$ provides a single-branch dispersion relation in the extended zone scheme for electrons represented by the dominant FLAPW wave function outside the MT potential. The value of *e*/*a* can be evaluated from the value of $\{2k_G(E)\}^2$ at E_F, since it would directly correspond to the square of the diameter of the Fermi sphere.

As emphasized in Ref. 14, the evaluation of the variance $\sigma^2(E)$ is critically important in the analysis, since $\{2k_G(E)\}^2$ is a quantity averaged over selected electronic states in the Brillouin zone. It is defined as

$$\begin{aligned}\sigma^2(E) &= [2\{k_G(E) + \sigma_G(E)\}]^2 - \{2k_G(E)\}^2 \\ &= 8k_G(E)\sigma_G(E) + 4\sigma_G(E)^2,\end{aligned} \tag{8}$$

where the standard deviation $\sigma_G(E)$ is defined as

$$\sigma_G(E) \equiv \sqrt{\sum_i \omega_i (|\mathbf{k}_i + \mathbf{G}|_E - k_G(E))^2}. \tag{9}$$

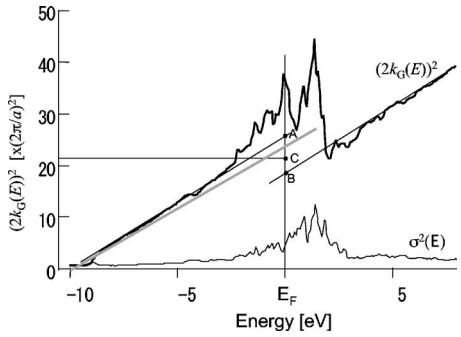

FIG. 14. Energy dependence of $\{2k_G(E)\}^2$ and its variance $\sigma^2(E)$ calculated from Eqs. (7)–(9) for the Al_8V_5 γ-brass. The square of the Fermi diameter is determined by taking a mean value of "A" and "B" intersecting of two straight lines with the Fermi level. The gray line refers to the free-electron model.

Figure 14 shows the energy dependence of $\{2k_G(E)\}^2$ for the Al_8V_5 γ-brass, along with that of the variance $\sigma^2(E)$. We consider the value of $\{2k_G(E)\}^2$ to become meaningless, when $\sigma^2(E)$ becomes significant. This happens in the energy range from −3 to +3 eV, where the V 3*d* states are located. This obviously indicates that the determination of e/a for this system is inherently difficult. Nevertheless, we attempted to estimate the e/a value in this system while keeping this dilemma in mind. The data outside ±3 eV range, where V 3*d* states become negligibly small, may be well fitted to two independent straight lines, as shown by solid lines in Fig. 14. The square of the Fermi diameter $\{2k_F\}^2$ is determined to be 21 by taking the mean value of "A" and "B" at the intersection of the two lines with the Fermi level. This is marked as "C" in Fig. 14. It is interesting to note that the value thus obtained is in good agreement with the value derived when U_{av} crosses the Fermi level in Fig. 6.

The effective e/a value for the Al_8V_5 γ-brass is then calculated to be 1.94 by inserting $\{2k_F\}^2=21$ into the relation $e/a=8\pi k_F^3/3N$, where N is the number of atoms in the unit cell equal to 52 and the Fermi wave number k_F is in units of $2\pi/a$. The e/a value of 1.94 is obviously much larger than the magic number of $21/13=1.615$ characterizing the stability of the prototype γ-brasses.[10,13–15] The effective e/a value for the V atom is deduced to be 0.23 from the total $e/a=1.94$ by assuming the valency of Al to be 3.

The value may be compared with those for other γ-brasses:[14,15] 0.96, 0.97, 0.15, 0.07, −1.7, and −2.5 for the e/a value of Cu in Cu_5Zn_8, Cu in Cu_9Al_4, Ni in Ni_2Zn_{11}, Pd in Pd_2Zn_{11}, Co in Co_2Zn_{11}, and Fe in Fe_2Zn_{11} γ-brasses, respectively. Among them, a comparison with Co and Fe is particularly interesting, since negative e/a values were assigned to them in contrast to the positive number in the present Al_8V_5 γ-brass. Here the negative e/a values for Co and Fe were deduced by taking into account only the data near the Fermi level in the energy dependence of $\{2k_G(E)\}^2$.

As discussed above, the variance in Al_8V_5 remained high in the energy range including the Fermi level, across which the V 3*d* states exist. Hence, we had to employ the data in the region outside the V 3*d* states. To maintain consistency among the results, we re-evaluated the e/a value of Co and Fe in Co_2Zn_{11} and Fe_2Zn_{11} by avoiding the use of the data, where Co 3*d* and Fe 3*d* states exist, in the same manner as that adopted in the present analysis. The values turn out to be +0.26 and +0.70 for Co and Fe, respectively. All the results thus obtained are listed in Table I, together with those reported in Ref. 14.

The assessment of the valency of the transition metal element has been controversial for many years. Raynor[21] assigned negative valencies to Cr, Mn, Fe, Co, and Ni by assuming that $CrAl_7$, $MnAl_6$, $FeAl_3$, Co_2Al_9, and $NiAl_3$ compounds are stabilized at a common e/a value of 2.1. The physical meaning for assigning negative valencies to the TM elements has been discussed elsewhere.[22,23] In contrast, there also exist reports, in which use of positive e/a values is more appropriate. Haworth and Hume-Rothery[24] assigned positive valencies of 1.8, 1.0, 0.8, and 0.6 for Mn, Fe, Co, and Ni so as to meet the phase boundary of the α- to $\alpha+\beta$-phases in Cu-*TM*-Zn and Cu-*TM*-Al ternary alloys at the same e/a value. Mizutani *et al.*[12] evaluated the effective e/a value of Ru in the Al-Cu-Ru-Si approximant to be 0.76 by applying the Hume-Rothery electron concentration rule under the assumption that the Fermi surface comes closest to {543}, {710}, and {550} zones and that Cu, Al, and Si donate one, three, and four electrons per atom, respectively. Ishimasa *et al.*[25] pointed out that the use of positive valencies proposed by Haworth and Hume-Rothery brings the stability range of their newly discovered Sc-*TM*-based quasicrystals to a universal e/a value of around 2.1.

We proposed in the present work the possession of small positive valencies for all TM elements by casting the FLAPW-derived electronic structure into the framework of the free electron model while preserving overall band fea-

TABLE I. $(2k_F)^2$, $(e/a)_{\text{total}}$, and $(e/a)_{\text{TM}}$ values for different γ-brasses.

	γ-brass						
	Al_8V_5	Fe_2Zn_{11}	Co_2Zn_{11}	Ni_2Zn_{11}	Pd_2Zn_{11}	Cu_5Zn_8	Cu_9Al_4
$(2k_F)^2$	21.0	20.0	19.5	19.36	19.27	18.47	18.45
Zones	$14 \leqslant G^2 \leqslant 30$	Not studied	Not studied	$G^2=18$ {411}, {330}	$G^2=18$ {411}, {330}	$G^2=18$ {411}, {330}	$G^2=18$ {411}, {330}
$(e/a)_{\text{total}}$	1.94	1.80	1.73	1.72	1.70	1.60	1.60
$(e/a)_{\text{TM}}$	0.23	0.70	0.26	0.15	0.07	0.96	0.97
Ref.	Present	Present	Present	14	14	14	14

tures deduced from the *ab initio* electronic structure calculations. The assignment of a small but positive valency for TM elements like the V atom means that TM elements are capable of increasing the number of mobile electrons in the interstitial region. In contrast, a negative valency assigned to the TM element means a transfer of mobile electrons donated by its partner element like Al from the interstitial region to the region inside the MT potential.

F. bcc to γ-brass phase transformation

As mentioned in the Introduction, the structurally complex γ-brass is constructed by a slight modification of the bcc structure. It is, therefore, of particular interest to shed more light on the phase transformation between these two phases. Our previous work on the Cu_5Zn_8 and Cu_9Al_4 γ-brasses[13] proved that the Fourier component of the FLAPW wave function at energies responsible for the formation of the pseudogap is extremely strong only at $|\mathbf{G}|^2=18$, i.e., the center of {411} and {330} zones. This naturally led to the supposition that they would best stabilize at the e/a value of 21/13 as a line compound. However, the γ-brass phase has a sizable solid solution range in both Cu-Zn and Cu-Al equilibrium phase diagrams.[1] At this stage, it may be worthwhile noting that the number of atoms in the unit cell decreases with increasing Al concentration beyond 35 at. % Al in the Cu-Al γ-brass phase field.[26] Hence, the FsBz interaction associated with the {411} and {330} zones can remain active in the Al-rich side, provided that the decrease in the number of atoms in its unit cell compensates for an increase in the number of electrons due to an increase in Al concentration so as to keep the number of electrons per unit cell unchanged.[26,27] However, we consider more elaborate work to be needed to explain the existence of a solid solution range in both Cu-Al and Cu-Zn alloy systems.

In the present Al_8V_5 γ-brass, we emphasized that all zones in the range $14 \leqslant |\mathbf{G}|^2 \leqslant 30$ harmoniously resonate with mobile electrons to form a wide pseudogap in the *sp*-partial DOS. The interpretation based on the V 3*d* states mediated resonance does not specify the particular zones and, hence, would not rule out the possession of a solid solution range around the stoichiometric composition of Al_8V_5. However, the γ-brass exists only as a line compound in the Al-V equilibrium phase diagram.[1] The atom size difference between Al and V is only 5.7%. Hence, its existence as a line compound is more difficult to understand and is beyond the level of our present understanding.

The Mott and Jones theory claims that an increase in electron concentration from 3/2 to 21/13 enables the bcc to γ-brass transformation by adjusting the expanding free electron Fermi sphere to the set of larger zones with $|\mathbf{G}|^2=18$, i.e., {330} and {411} zones in place of the set of {110} zones with $|\mathbf{G}|^2=2$ for the bcc. If we assign the e/a value of 0.23 to both bcc $Al_{54}V_{46}$ and Al_8V_5, their electron concentrations turn out to be 1.73 and 1.94, respectively. Thus, the phase transformation from the bcc to γ-brass in the Al-V system is brought about by an increase in the electron concentration in the same way as that in the Cu-Zn system. Judging from the discussion above, however, we consider it not to be legitimate at the moment to discuss the phase transformation in the system characterized by the *d* states mediated resonance in line with the naïve Mott and Jones theory.

V. CONCLUSIONS

By making full use of the advantage of two different first-principles electronic structure calculations, FLAPW and LMTO-ASA, we attempted to gain a deeper insight into why the Al_8V_5 γ-brass can be stabilized by accommodating 52 atoms in its unit cell. The LMTO-ASA calculations could identify a deep valley at 0.5 eV above the Fermi level in the DOS as arising from orbital hybridizations between the V 3*d* and Al 3*p* states. On the other hand, the FLAPW electronic structure calculations revealed the V 3*d* states mediated resonance of mobile electrons with different sets of lattice planes including not only $|\mathbf{G}|^2=18$ corresponding to {330} and {411} planes but also those in the range $14 \leqslant |\mathbf{G}|^2 \leqslant 30$. The electronic structure of the CsCl-type AlV compound was also calculated in the context of the FLAPW and LMTO-ASA methods. It turned out that the V 3*d* mediated resonance is unique only for a large unit cell system, where sets of lattice planes in a wide range of $|\mathbf{G}|^2$ can participate with the assistance of the V 3*d* states, which serves as a source supplying high reciprocal lattice vectors, i.e., high momentum transfer vectors. The resonance effect is found to play a key role in condensing the bonding states below the Fermi level to gain electronic energy in the Al_8V_5 γ-brass.

ACKNOWLEDGMENT

One of the authors (U.M.) is grateful for the financial support of the Grant-in-Aid for Scientific Research (Contract No. 17560583) from the Japan Society for the Promotion of Science.

[1] H. Okamoto, *Phase Diagrams for Binary Alloys* (ASM International, OH, 2000).
[2] A. J. Bradley and J. Thewlis, Proc. R. Soc. London, Ser. A **112**, 678 (1926).
[3] J. K. Brandon, W. B. Pearson, P. W. Riley, C. Chieh, and R. Stokhuyzen, Acta Crystallogr., Sect. B: Struct. Crystallogr. Cryst. Chem. **33**, 1088 (1977).
[4] O. v. Heidenstam, A. Johansson, and S. Westman, Acta Chem. Scand. (1947-1973) **22**, 653 (1968).
[5] J. K. Brandon, R. Y. Brizard, P. C. Chieh, R. K. McMillan, and W. B. Pearson, Acta Crystallogr., Sect. B: Struct. Crystallogr. Cryst. Chem. **30**, 1412 (1974).
[6] A. J. Bradley and P. Jones, J. Inst. Met. **51**, 131 (1933).
[7] A. F. Westgren and G. Phragmen, Trans. Faraday Soc. **25**, 379 (1929).
[8] N. F. Mott and H. Jones, *The Theory of Properties of Metals and*

Alloys (Dover, New York, 1958), pp. 168–174.
[9] T. B. Massalski and U. Mizutani, Prog. Mater. Sci. **22**, 151 (1978).
[10] U. Mizutani, in *The Science of Complex Alloy Phases*, edited by T. B. Massalski and P. E. A. Turchi (The Minerals, Metals & Materials Society, Warrendale, PA, 2005), p. 1.
[11] A. T. Paxton, M. Methfessel, and D. G. Pettifor, Proc. R. Soc. London, Ser. A **453**, 1493 (1997).
[12] U. Mizutani, T. Takeuchi, and H. Sato, Prog. Mater. Sci. **49**, 227 (2004).
[13] R. Asahi, H. Sato, T. Takeuchi, and U. Mizutani, Phys. Rev. B **71**, 165103 (2005).
[14] R. Asahi, H. Sato, T. Takeuchi, and U. Mizutani, Phys. Rev. B **72**, 125102 (2005).
[15] U. Mizutani, R. Asahi, H. Sato, and T. Takeuchi, Philos. Mag. **86**, 645 (2006).
[16] O. N. Carlson, D. J. Kenney, and H. A. Wilhelm, Trans. Am. Soc. Met. **47**, 520 (1955); W. B. Pearson, *Handbook of Lattice Spacing and Structures of Metals and Alloys* (Pergamon, London, 1958).
[17] H. Sato, T. Takeuchi, and U. Mizutani, Phys. Rev. B **64**, 094207 (2001).
[18] H. Sato, T. Takeuchi, and U. Mizutani, Phys. Rev. B **70**, 024210 (2004).
[19] E. Wimmer, H. Krakauer, M. Weinert, and A. J. Freeman, Phys. Rev. B **24**, 864 (1981).
[20] M. Weinert, E. Wimmer, and A. J. Freeman, Phys. Rev. B **26**, 4571 (1982).
[21] G. V. Raynor, Prog. Met. Phys. **1**, 1 (1949).
[22] G. Trambly de Laissardiere, D. N. Manh, L. Magaud, J. P. Julien, F. Cyrot-Lackmann, and D. Mayou, Phys. Rev. B **52**, 7920 (1995).
[23] E. S. Zijlstra and S. K. Bose, Philos. Mag. **86**, 717 (2006).
[24] J. B. Haworth and W. Hume-Rothery, Philos. Mag. **43**, 613 (1952).
[25] T. Ishimasa, S. Kashimoto, and R. Maezawa, Mater. Res. Soc. Symp. Proc. **805**, 3 (2004).
[26] W. Hume-Rothery, J. O. Betterton, and J. Reynolds, J. Inst. Met. **80**, 609 (1951–1952).
[27] T. Takeuchi, T. Onogi, E. Banno, and U. Mizutani, Mater. Trans. **42**, 933 (2001).